Global NEST Journal, Vol 26, No 9, 06479

Biosorption of Pb(II) ions through nanostructured teff straw based magnetized activated biocarbon: Aspects on modeling, optimization, and kinetics

Mohanasundaram Sugumar[1], Selvaraj Bharathi[2], Venkatesan Sampath[3], Venkatesa Prabhu Sundramurthy[4,5]*, Mayakannan Selvaraju[6], Shine Kadaikunnan[7] and Jamal Mohammed Khaled[7]

[1]Department of Biochemistry and Crop Physiology, SRM College of Agricultural Sciences, SRM Institute of Science and Technology, Baburayanpettai – 603201, Maduranthagam Taluk, Chengalpattu District, Tamil Nadu, India.
[2]Department of Research Analytics, Saveetha Dental College and Hospitals, Saveetha Institute of Medical and Technical Sciences, Saveetha University, Chennai – 600 007, India
[3]Department of Biochemistry, Sri Sankara Arts and Science College (Autonomous), Enathur, Kanchipuram - 631561, Tamil Nadu, India.
[4]Centre for Natural Products and Functional Foods, Karpagam Academy of Higher Education, Coimbatore, 641 021, Tamil Nadu, India.
[5]Department of Biotechnology, Faculty of Engineering, Karpagam Academy of Higher Education, Coimbatore -641 021, Tamil Nadu, India.
[6]Department of Mechanical Engineering, Rathinam Technical Campus, Coimbatore – 641021, Tamil Nadu, India.
[7]Department of Botany and Microbiology, College of Science, King Saud University, P. O. Box 2455, Riyadh 11451, Saudi Arabia.
Received: 18/07/2024, Accepted: 25/09/2024, Available online: 16/10/2024
*to whom all correspondence should be addressed: e-mail: haiitsvp@gmail.com
https://doi.org/10.30955/gnj.06479

Graphical abstract

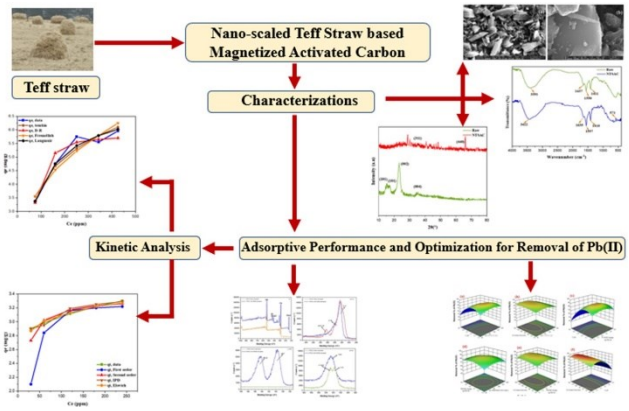

Abstract

In this study, activated carbon (AC) was prepared from teff grass straw via chemical activation and microwave-assisted pyrolysis. The AC was modified by magnetization followed by it was characterized by particle size, FTIR, XRD, thermogravimetric study, pore size, and magnetic properties. Further, it was evaluated for its adsorptive removal performance of lead (II) ions from aqueous solution. A statistical model was developed by response surface method (RSM) and the crucial parameters, concentration of initial Pb(II), biosorbent loading, solution pH, and contact time were optimized for maximizing the adsorption of Pb(II) ions. The optimal values were 95.36 mg/L, 0.656 g/100 mL, 5.5, and 88.7 min, respectively for aforementioned parameters. Under the optimal condition, the Langmuir isotherm exhibited the most accurate correspondence with the obtained experimental data. The findings from the kinetic analysis were found to be statistically fit to the pseudo-2nd order model.

Keywords: Adsorption, isotherm, kinetics, magnetized biocarbon, optimization, Pb(II), and teff straw.

Abbreviations

%	Percentage
°C	Degree Celsius
AAS	Atomic absorption spectrometry
ABC	activated carbon
CCD	Central composite design
FTIR	Fourier transform infrared spectroscopy
Ml	Milliliter
NTSAC	Nano-structured teff straw based activated carbon
Pb(II)	Lead(II) ions
pH	Potential of hydrogen
SEM	Scanning electron microscopy
TS	Teff straw
XRD	X-ray diffraction

1. Introduction

The need of clean water is under increasing threat due to pollution caused by industrial, residential, and agricultural practice (Rahman *et al.* 2021). Wastewaters that properly untreated before being released into the environment should be concerned seriously because it causes inadequate hygiene services which is highly endangers to natural ecology due to different contaminants (Naidu *et al.* 2021). Among these contaminants, heavy metal ions are

considered as extremely hazardous since they combine with other environmental components like soil, water, or air and can expose to humans and other living things through the food chain (Qasem *et al.* 2021). They mainly come from the manufacturing process, particularly, paint factories, tanneries, battery plants, and other refineries. In this regard, lead [Pb(II)] is one of the most dangerous heavy metal pollutants because it can cause a wide range of health problems in humans, including dizziness, headaches, nausea, and stomach problems (Balasubramanian *et al.* 2020). Unlike other metals like zinc, copper, and manganese, which have biological purposes, lead is a poisonous heavy metal that seriously interrupts several biological functions in plants and animals (Levin *et al.* 2021). Lead's damaging effects have been subjected of numerous researches, and one of these used the Microtox Assay to compare and contrast the relative toxicity of other metals (Kumar *et al.* 2022). According to the World Health Organization, 0.01 mg/L is the absolute maximum level of Pb that should be present in drinking water. Hence, necessary precautions to safeguard the people from Pb(II) exposure is extremely crucial in order to prevent harmful impacts (Raj and Das 2023). Keeping view in this concern, many kinds of wastewater treatment have been developed to get rid of Pb(II) and its the harmful effects, such as chemical precipitation, adsorption, filtration, ion exchange membrane separation, coagulation, and osmosis.

However, heavy metals, like Pb are difficult and expensive to remove on a large scale, and current methods are inefficient, complicated, and not very selective. In contrast, adsorption technique using biosorbents is low expensive method and its effectiveness has made it a well-recognized approach for the removal of many heavy metals (Dąbrowski 2001). However, the selection of a suitable biosorbent play a crucial role with respect to adsorption efficiency, pollutant selectivity, reusability, and adsorption capacity for the intended use (Sharmiladevi *et al.* 2024). Accordingly, several heavy metals have all been researched using different range of biosorbents. Historically, the biosorbents derived from sugarcane bagasse, peanut shells, *Arundinaria alpina*, coffee husk, etc. have been well-proven to produce excellent results in removing heavy metals (Chen *et al.* 2020). Notwithstanding, preparation of green-based biosorbent material from agricultural residues gains significant attention that can be addressed by valorizing the agro-wastes. The possibility of using different bio-based adsorbents made from agricultural sources for the uptake of the hazardous metal elements have been documented elsewhere. According to previous studies, the adsorption capacity varies widely dependent on the nature of the bio-based absorbents and the type of heavy metal being absorbed (Ighalo and Adeniyi 2020).

In this line, the capacity of various materials for adsorbing Pb(II) from contaminated water has been investigated through the use of different biosorbent materials (Awad *et al.* 2020). In this light, activated carbon (AC) is one of the promising biosorbents that can be derived from lignocellulosic materials. According to Surafel *et al.* the AC derived from teff hay biomass has shown an excellent result for adsorptive removal of Pb(II) ions from aqueous solution (Beyan *et al.* 2024). At the optimum treatment condition, the authors observed a 99.8% Pb(II) removal by AC obtained from teff hay. In another study, the performance of titanate nanoflowers for adsorptive removal of Pb(II) and its process kinetics were examined by Huang *et al.* (Huang *et al.* 2012). According to them, titanate nanoflowers exhibited promising results for Pb(II) removal and it was observed that the pseudo-2nd order kinetics and the Langmuir isotherm have provided an exceptional fit to the experimental data. Hu and Shipley carried out an adsorption study using TiO_2 nanoparticles. They found that the adsorption efficacy around 95% after a fourfold regeneration cycle at an optimal pH of 2 (Hu and Shipley 2012).

Similarly, biosorbents were prepared from avocado seeds and used to effectively remove chromium and lead from aqueous solution (Aiyesanmi *et al.* 2022). Both the natural and chemically activated adsorbents had shown removal efficiencies of over 80% of heavy metal at the operating temperature 45°C and solution pH 5 (Leite *et al.* 2018). In study elsewhere, Ameen *et al.* prepared biochar from the agricultural wastes of palm to examine the adsorption competence of copper and lead (Ameen *et al.* 2022). They reported that the adsorption of 99 mg/g was determined to be the maximized adsorption capacity for Pb(II) by the developed biochar material. By altering several operating settings, Bagali *et al.* investigated the kinetics of the adsorption of Pb(II) ions while using a banana's pseudo-stem derived AC (Bagali *et al.* 2017). Recently, researchers have synthesized an inexpensive and environmentally friendly solid-phase AC made from coffee husk waste. It allowed for a maximum removal of 98% Pb(II) with an adsorption capacity of 19 mg/g (Gonçalves *et al.* 2013a). Though several authors have mentioned different types of agricultural waste in their AC formulations for removal of lead, utilization of teff straw has not been studied extensively and still it is underutilized for biosorbents preparation (Kifetew *et al.* 2023). The agricultural residue, teff straw (TS) is a common and naturally occurring lignocellulosic waste in Ethiopia (Sundramurthy *et al.* 2024).

The teff plant accounted for about 25% of Ethiopia's total harvest, making it the country's most important agricultural residue. The teff plant is considered agricultural trash once the seed has been harvested. Bio-based AC/adsorbent can be less expensive to produce than the adsorbent made from more expensive precursors, given that lignocellulosic material, TS, has no economic usefulness and is merely undesirable solid waste (Tessema *et al.* 2023). So, the originality of this study is in its use of preparing activated carbon from TS to propose remediation measures for Pb(II) removal from wastewater.

In this study, a chemical activation method was adopted to prepare AC using TS, which was then subjected to magnetization. Because of their exceptional adsorption capacity and strong magnetism property, magnetic adsorbents gain more attention in treating environmental contamination. Furthermore, the prepared adsorbent was evaluated for adsorption removal capability of Pb(II) ions

by batch mode. Response surface method (RSM) in conjunction with the central composite design (CCD) was utilized to improve the absorption efficiency. Additionally, the kinetics, isotherm model, and thermodynamic investigations were evaluated using the adsorption data. Furthermore, desorption and regeneration studies were also performed to explore more about the adsorptive-potential of prepared adsorbent for its reuse.

2. Experimental methodology

2.1. Materials

TS was obtained on farmland in Addis Ababa, Ethiopia, after the teff seeds had been harvested during the month of March 2022. TS sample has been transported to SRM Institute of Science and Technology, India using airtight containers to carry out the experiments. The TS was washed multiple times with tap water and then with deionized water to eliminate dust and other contaminants before being dried in an oven set to 65°C for two days. To acquire the necessary particle size for this investigation, it was first pulverized and then sieved. For experimentation, distilled water, zinc chloride ($ZnCl_2$), potassium nitrate (KNO_3), sodium chloride (NaCl), and lead nitrate [$Pb(NO_3)_2$] were utilized. Hydrochloric acid and Sodium hydroxide were employed to achieve the desired pH level. An atomic absorption spectrophotometer (AAS) (PerkinElmer, Model-PINAACLE 900T) was utilized in accordance with standard protocols to ascertain the quantity of Pb(II) ions.

2.2. AC preparation, Magnetization, and Nano-biocarbon Preparation

Initially, the TS powder was subjected to impregnation with $ZnCl_2$ (1:1 ratio), then, the activated carbon was produced by microwave pyrolysis technique (Oliveira *et al.* 2009). After impregnation, a homogenous paste was made by blending the with 0.05L of sterile water. The paste that formed was placed in a quartz container for pyrolysis with 2.5 mL/sec of inert N_2 gas. Microwave pyrolysis facilitates more extensive pyrolysis decomposition compared to the conventional pyrolysis. It is a thermochemical technique, which makes use of electromagnetic waves with the dipoles that interact with the heated material. As a result, heat is created inside the target material rather than coming from an outside source, which makes the heating process easier to manage and more efficient in terms of uniform heat distribution. After the pyrolysis, a flow of inert N_2 at 2.5 ml/sec was used to cool the sample. Then, the resulted material was immersed in a solution of distilled water and hydrochloric acid (1:1) at 85°C for 120 min. The sample matrix had inorganic chemicals leached out throughout this process (Zhao *et al.* 2022). Excessive washing with distilled water was applied to resultant carbonaceous materials until the washing water's pH reached to 7. Next, it was subjected to a drying process in an oven set at 85°C with a constant airflow for a duration of 12 h.

Magnetization of AC has been prepared using a solution containing 2:1 molar ratio of Fe^{3+}/Fe^{2+}. For this purpose, a solution containing 5.03 g $FeCl_3.6H_2O$ and 5.2 g $FeSO_4.7H_2O$ in 100 mL of distilled water (Varadharajan *et al.* 2022). The mixture was well stirred by for 15 min. Then, prepared AC (5 g) was supplemented followed by the mixture was stirred for 20 min. During this time, the solution was maintained at 60°C. Moreover, the slurry mixture was lowered in temperature to 35 °C. Then, the necessary amount of sodium hydroxide (5 mol/L) was added to the solution to bring the solution pH level down to 10. A magnetic field was applied to separate the magnetized AC that had been mixed continuously for 8 h. Further, it was cleaned with ethanol. A vacuum drier was used to dry the obtained magnetized AC sample, and then it was sealed in an airtight container. It was kept in a cool, dry environment. Additionally, in order to achieve nanostructured material, the particle size was reduced using ball milling technique. Ball milling is one of the oldest and most reliable ways to make nanostructured materials. In this study, planetary centrifugal ball mill was used. For grinding purpose, stainless steel balls (no of balls, 800; radius, 1.3 mm; total weightage of the balls, 50 g) were utilized in this experiment. To prevent the balls and biocarbon from overheating, 5-minute on/off timing of the ball milling experiment was carried out. Using laser beam scattering equipment, the mean and distribution of particle size the biocarbon sample was assessed after 14 h of milling. Particle size distribution was determined by combining 1 mg of activated biocarbon with 0.5% Tween 80 and 1% ethanol in 200 mg of distilled water for 50 min with the use of a magnetic stirrer.

2.3. Characterization of Nano-structured Teff Straw based Activated Carbon (NTSAC)

The physical-chemical properties of the NTSAC sample were analyzed for its characteristics by following the procedures set out by the ASTM standard. To measure the point of zero charge (pzc), the method reported by Kifetew *et al.* (Merine *et al.* 2024) was followed.

Further, surface morphology and elemental composition were examined using field emission scanning electron microscopy (FESEM, QUANTA-250 FEG) and EDX (Bruker Xflash 6130) techniques, respectively. The crystalline nature of the synthesized sample was analyzed with the help of X-ray powder diffraction (XRD, Rigaku ULTIMA-IV). A Scherrer's equation [Equation (1)] was used with XRD data to determine crystallinity (Igalavithana *et al.* 2017). Fourier transform infrared spectroscopy (Bruker Tensor 27) at 400-4,000 cm^{-1} was used to determine the available functional groups of NTSAC. The utilization of the BET (Brunauer-Emmett-Teller) technique, which measures the nitrogen adsorption capacity of NTSAC at 77 K, the surface area, pore size distribution, and pore volume were found using a BET instrument (Microtrac BELSORP-mini II).

$$\text{Crystallinity} = \frac{\text{Crystalline peaks area}}{\text{All peaks area}\left(\text{amorphous} + \text{crystalline}\right)} \times 100 \quad (1)$$

2.4. RSM-based statistical analysis on lead (II) adsorption

The effectiveness of adsorption process depends on several independent variables, such as adsorbent type and amount, the process temperature, the stirring speed,

particle size of the adsorbent, the processing time, and the solution pH (Tee *et al.* 2022). In research elsewhere, with aiming to enhance the adsorptive removal of Pb(II) ion by the selective adsorbent, optimal circumstances have been identified by multiple researchers. In the present study, the influence of independent factors, the initial concentration of Pb(II) ions, adsorption period, solution pH, and dosage of NTSAC were considered to investigate by a batch-based adsorption study. For adsorption experiments, a conical beaker (0.1 L volume of each sample) with a thermostatic stirrer set to room temperature was operated with 200 rpm shaking speed. Clear liquid was obtained by filtering the mixture through Whatman No. 1 filter paper, and then the amount of Pb(II) ion residue was determined using atomic absorption spectrometry (AAS) at 217 nm. A blank solution was also analyzed alongside each sample. Equation 2 was employed to compute the percent removal of Pb(II) adsorption by NTSAC subsequent to the determination of the adsorption capacity (Equation 2) (Jagadeesh and Sundaram 2023).

$$\text{Efficacy Removal}(\%) = \frac{C_o - C_f}{C_o} \times 100 \quad (2)$$

$$Q\left(\frac{mg}{g}\right) = \frac{C_o - C_f}{m} \times V \quad (3)$$

Where, C_o is initial Pb(II) concentration in mg/l, C_f is final Pb(II) concentration in mg/l, m is adsorbent mass in g, V is volume of the solution in ml.

In the present study, the optimum value for the chosen independent parameters, namely, NTSAC dose, adsorption time, pH, and initial concentration of Pb(II) were statistically analyzed for maximizing Pb(II) removal from the synthetic solution. During experimentation, the agitation speed was maintained at a constant rate of 200 rpm, while the temperature was held at room temperature. Response surface methodology (RSM) is a statistic technique which is used for interaction investigation and to optimize process parameters. When designing experiments, RSM approach is frequently employed to reduce the number of trials for a given number of parameters and their values. Herein, the RSM analysis was carried out using selected variables that were chosen to optimize by grouping via central composite design (CCD) approach. It guarantees a comprehensive analysis of all pertinent components and their interrelationships. With their corresponding levels, the chosen variables are listed in **Table 1**. CCD suggested a series of 30 trials according to the limitations figure, validate axial, factorial, and average levels. Consequently, the average adsorption was considered value by looking at each experiment three times. Using RSM analysis a polynomial equation model (Equation 4) was constructed that describes the relation between the experimental response and the chosen parameters.

$$R = \theta_0 + \sum_{j=1}^{4}\theta_j Y_j + \sum_{j=1}^{4}\theta_{jj} Y_j^2 + \sum_{i}\sum_{<j=2}^{4}\theta_{ji} Y_i Y_j + e_i \quad (4)$$

Where, R is response [(%) removal of Pb(II)], θ_0 refers the intercept coefficient, e_i is known as correlation error.

In addition, statistical optimization was used on the process variables with the aim of maximizing the Pb(II) removal. All statistical restraints were evaluated with ANOVA (analysis of variance). The optimum values were determined by solving the regression equation containing the selected variables. Using a response surface map, the interaction among the factors were analyzed. In this regard, Design-Expert 12 was used to developed RSM and CCD probes. The created model was confirmed through a triple experimental run, as expected by the design expert (Duan *et al.* 2023).

Table 1. Input factors and its levels for biosorption study

Factors	Factor coding	Unit	-α	-1	-1	+α
Initial Pb (II) concentration	A	mg/L	20	60	140	180
NTSAC dosage	B	g/100 ml	1	2	4	5
Contact time	C	min	30	60	90	150
Solution pH	D	–	1.5	2	3	3.5

Table 2. Results on proximate analysis for NTSAC sample.

Biomass	HY (%)	FCC (%)	A (%)	C (Mc/cm)	MC (%)	CY (%)	BD (g/cm^3)	VM (%)	SA (m^2/g)	P_{ZC}	pH
NTSAC	4.62	69.74	5.03	0.61	5.78	65.18	0.76	18.42	494.2	4.86	7.15

Where, HY - hydrogen yield; FCC - fixed carbon content; C - conductivity; A - ash content CY- carbon yield; VM - volatile matter; SA - surface area; MC - moisture content; P_{ZC} - point zero charge; BD - bulk density

2.5. Equilibrium adsorption studies

The experimental findings were correlated and the adsorption mechanisms were evaluated using the adsorption isotherm models, namely, Freundlich, Temkin, Dubinin - Radushkevich (D-R) and Langmuir (Rose *et al.* 2023). Langmuir isotherm model evaluates the monolayer adsorption on a uniform adsorbent surface, where the adsorption sites are all the same and have the same adsorption energy. The equations, (5) and (6), reflect the linear and nonlinear Langmuir models, correspondingly (Mohammadpour *et al.* 2023).

$$\frac{C_e}{q_e} = \frac{1}{q_m k_L} + \frac{C_e}{q_m} \quad (5)$$

$$q_e = \frac{q_m k_L C_e}{1 + k_L C_e} \quad (6)$$

Here, q_e (mg/g) is amount of Pb ions adsorbed by an equilibrium mass of adsorbent, q_m (mg/g) denotes the Pb

ion monolayer formation capacity at maximal adsorption capacity as a function of adsorbent mass, C_e (mg/L) is the equilibrium Pb ions in in the aqueous solution. k_L (L/mg) refers the adsorption energy which is a constant for the Langmuir isotherm.

The Freundlich model relies on the fact that adsorbent surfaces are typically not perfectly smooth, and that different adsorption sites have variable enthalpies of adsorption. Equations (7) and (8) can be used to depict the Freundlich isotherm (Karuppaiyan *et al.* 2023).

$$\ln q_e = \frac{1}{n}\ln C_e + \ln k_f \quad (7)$$

$$q_e = k_f C_e^{1/n} \quad (8)$$

Herein, k_f denotes the adsorption capacity; n refers the non-linearity of the function. The factors, n and k_f, can be computed using the plot developed from the ln(q_e) versus ln(C_e).

When assessing the possibility for adsorbate/adsorbent interactions, the Temkin (T) isotherm can be used to measure the interface between ion concentrations. The Temkin isotherm model can be represented by the equations (9) and (10) (Karuppaiyan *et al.* 2023).

$$q_e = \frac{RT}{b}\ln\left(AC_e\right) \quad (9)$$

$$q_e = \frac{RT}{b}\left[\left(\ln k_T + \ln\left(C_e\right)\right)\right] \quad (10)$$

Herein, b and K_T (L/mol) are the Temkin constants, b is adsorption of heat constant (J/mol), T refers absolute temperature constants (K), R is gas constant (8.314 J/mol K).

The D-R model performs exceptionally well in the concentration range of medium to high concentrations because of this model well-correlates the multilayer adsorption property due to physical adsorption. The equations, (11) and (12) represent the D-R model (Zhang *et al.* 2024).

$$\ln q_e = \ln q_m - k_D\varepsilon^2 \quad (11)$$

$$\text{Where, } \varepsilon = RT\ln\left(1+\frac{1}{C_e}\right) \quad (12)$$

where, k_D (mol^2/kJ^2) is a constant proportional to the enthalpy of adsorption, ε Polanyi potential that can be obtained from equation (12), E (kJ/mol) is free energy (kJ/mol). This represents the adsorption energy that can be determined by the equation (13) using the value of k_D.

$$E = \frac{1}{\sqrt{2K_D}} \quad (13)$$

2.6. Kinetic Approaches on Adsorption

To conduct the kinetic analysis, 5 g of adsorbent was used. The experiment solution contained 0.1 L of 100 ppm Pb(II) ions supplemented with 5 g of NTSAC. The mixture was continuous agitated at 250 rpm for required time. In the first half an hour, aliquots were taken at regular intervals of 5 min due to the rapid adsorption process preceding saturation. Then, for the next 5 hours, the samples were taken at the 60-min mark. To assess their suitability for the kinetic data, various models were evaluated, such as pseudo-1st order, pseudo-2nd order, Elovich kinetic, and intraparticle diffusion. The pseudo-1st-order and 2nd order kinetic models are described by the equations, (14) and (14), respectively (Cao *et al.* 2024).

$$\ln\left(q_e - q_t\right) = \ln\left(q_e\right) - k_1 t \quad (14)$$

where, q_t refers quantity of adsorbed Pb(II) at any time t (mg/g), q_e refers quantity of adsorbed Pb(II) at the equilibrium stage. k_1 refers the pseudo-1st-order kinetic constant (Debnath and Das 2023).

$$\frac{1}{q_t} = \frac{1}{k_2 q_e^2} + \frac{t}{q_e} \quad (15)$$

When the adsorption rate is controlled by the diffusion of adsorbate, the intra-particle diffusion kinetic model (equation 16) outperforms the other models while fitting the kinetic data. The significance of particle diffusion during adsorption can be explained by the linearity of the fitness function which defined by the intraparticle diffusion model (Danish *et al.* 2022).

$$q_t = k_{dif} t^{1/2} + C \quad (16)$$

While plotting 'q_t' *vs* '$t^{1/2}$', the width of the boundary layer (C) can be determined from the intercept value. This value is used to calculate the external mass transfer resistance.

Elovich kinetic is an additional prominent kinetic model that can be employed to analyze the kinetics and adsorption mechanism. The Elovich kinetic model is stated in its streamlined form by equation (17). According to this model of equation, the linear relationship between 'q_t' vs 'ln(t)' has a slope of (1/a_E) and an intercept of (1/a_E) ln ($a_E b_E$) (Al-Hazmi *et al.* 2024).

$$q_t = \frac{1}{a_E}\ln\left(b_E a_E\right) + \frac{1}{a_E}\ln\left(t\right) \quad (17)$$

Where, a_E is constant of desorption (g/mg); b_E denotes rate of initial adsorption (mg/min).

3. Results and discussion

3.1. Characteristics of NTSAC

3.1.1. Physiochemical characterization

The adsorption approach has certain limitations when it applies for removing heavy metals from aqueous solutions. Proximity analysis results for NTSAC and other agricultural biomasses are tabulated in **Table 2**. According to the NTSAC's physiochemical characterization, the percentage of fixed carbon was found to be high. These results were foreseen due to the presence of these elements in the cellulose, hemicellulose, and lignin molecules. In general, heavy metal removal by adsorption can be facilitated by materials rich in lignocellulosic content, which contain different functional groups including hydroxyl, amines, and carboxyl. The amount of water vapor present in a substance was characterized by its moisture content (MC). The MC, AC, and VM of obtained NTSAC sample, a porous material, were all found to be less. If the biocarbon sample

has a high ash content, it will have a low adsorption capability. There were fewer non-carbon components while compared to the primary carbon analogue. NTSAC qualities with a higher FCC and CY content might be claimed as graphitization grade. NTSAC's high CY and FCC content made it as a promising adsorbent candidate. NTSAC's FCC and CY were also noticeably higher than those of other lignocellulose-based ACs, like those made from corncob and coffee husk (Gonçalves *et al.* 2013b; Song *et al.* 2013). Bulk density (BD) value for agricultural waste adsorbent that is intended for use as AC should not exceed 0.25 g/cm^3. According to the results, the NTSAC's bulk density of 0.76 g/cm^3 made it met the previously mentioned requirement. pH has significant impact on the adsorption of Pb(II) ions by NTSAC. In this line, the it has been found that adsorbent can be effective at removing Cr^{6+}, Ni^{2+}, and Pb^{2+} since the biocarbon at pH value between 5.5 and 7.5. In addition, the resultant biocarbon sample has P_{ZC} value of 4.86, which promising that the lower P_{ZC} value is preferable with increased cation adsorption.

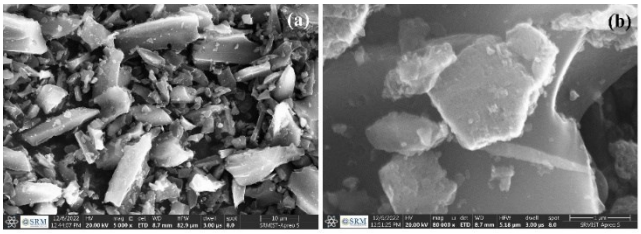

Figure 1. The SEM surface morphology of acquired NTSAC sample.

3.1.2. Surface morphology

The SEM has been used for many years to learn about the surface's shape and the adsorbent's structure. **Figure 1** depicts the SEM surface morphology of NTSAC sample. The surface morphology was observed to be uneven and harsh in its surface structure. These biochar pieces were found to be covered in aggregated particles after being magnetized. Following the magnetization process, the aggregates' coating took on a crystal flake-like form. The morphological shifts observed in materials treated with various iron salts have been confirmed by numerous researches. **Figure 2** illustrates the particle size distribution for the resultant NTSAC sample. Santhosh *et al.* found in magnetized biochar samples derived from sludge and woodchips structures resembling flake-shaped objects composed of aggregated Fe_2O_3 nanoparticles ranging in size from 50 to 100 nanometers (Santhosh *et al.* 2020). The authors, Guel-Nájar *et al.* who investigated the morphology of magnetized biochar prepared from corn straw, shown to a similar conclusion (Guel-Nájar *et al.* 2023). The flakes of nano-dispersed oxide phase that coat the biochar's pores and cavities increase its surface area and adsorption capability. According to Mohan *et al.* magnetized biochar made from oak wood and oak bark has shown increased the material's specific surface area (Mohan *et al.* 2014). However, after the TS was acid impregnated activation, a large number of pores were found in the NTSAC. High temperatures during processing damaged the lignocellulosic material, and the chemical vapors that were evaporated left the material with intact stomates. This porosity on the surface may have a crucial role in the binding of Pb(II) ions.

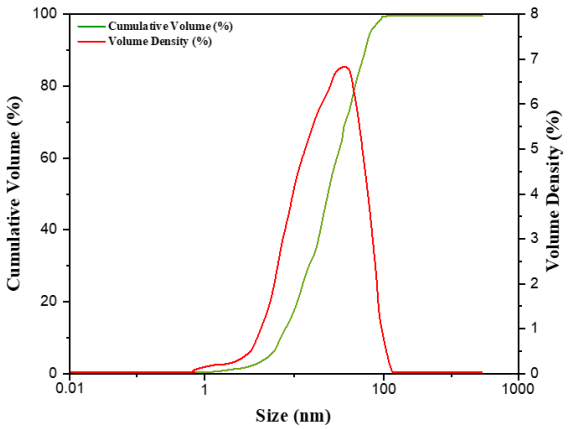

Figure. 2. Particle size distribution profile for resultant NTSAC sample.

3.1.3. FTIR analysis for Functional groups

The synthesized adsorbent materials' functional group content was examined by means of Fourier transform infrared spectroscopy (FTIR). **Figure 3** presents the FTIR spectra obtained from the samples of raw TS powder and NTSAC. The FTIR examination results showed that the raw material contained many different types of cellulose and organic functional groups. The stretching vibration of the O-H bond was amplified at 3394 cm^{-1}. The fainter peaks at 2946 cm^{-1} and 2872 cm^{-1} indicated the C-H stretching vibration for alkanes. Hydroxyl bending, C-O stretching, and aromatic C-C stretching were identified which attributed to the spectral peaks at 1639, 1552, and 1412 cm^{-1}, respectively (Dong *et al.* 2022). However, the FTIR spectra for magnetic biochar showed changes after biocarbon magnetization, specifically between 400 and 600 cm^{-1}. The Fe-O stretching mode in magnetite's octahedral and tetrahedral sites were indicated by a brief peak at 570 cm^{-1}. The absence of Fe(II) was indicated by the presence of weak absorption bands at 645cm $^{-1}$, 604 cm $^{-1}$, and 449 cm $^{-1}$.

The results revealed that the sample had signatures unique to lignocellulosic-based biochar. The FTIR spectrum of NTSAC was related to that of raw, and it was found that the intensity of various bands had decreased. This was especially true for the bands at 3391 cm^{-1} and 1637 cm^{-1}, as well as the bands at 1550 and 1411 cm^{-1}. The pyrolysis process has reduced the band intensities because several functional groups in the raw material's components were destroyed by microwave pyrolysis. For example, aliphatic hydroxyl groups in the biomass might subjected to thermal degradation between 120 and 200°C. At temperatures above 400°C, aliphatic methylene, methyl, and methoxy groups could be cleaved, and carboxyl and carbonyl groups were led to regenerate. Therefore, the synthesis of biochar with significant carbonization was confirmed by the attenuation of many peaks in the FTIR spectrum at 450°C.

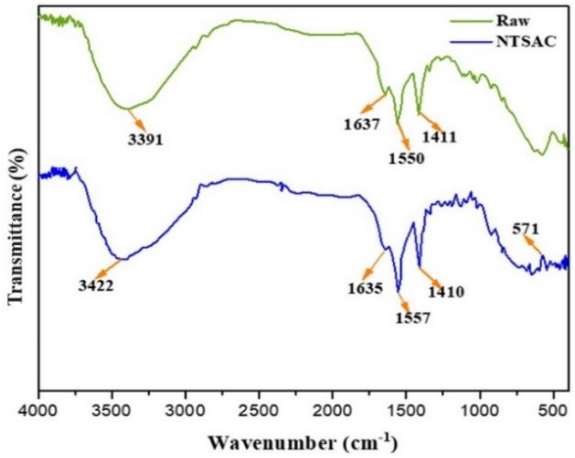

Figure 3. Spectra obtained from FTIR analysis of raw material and prepared NTSAC.

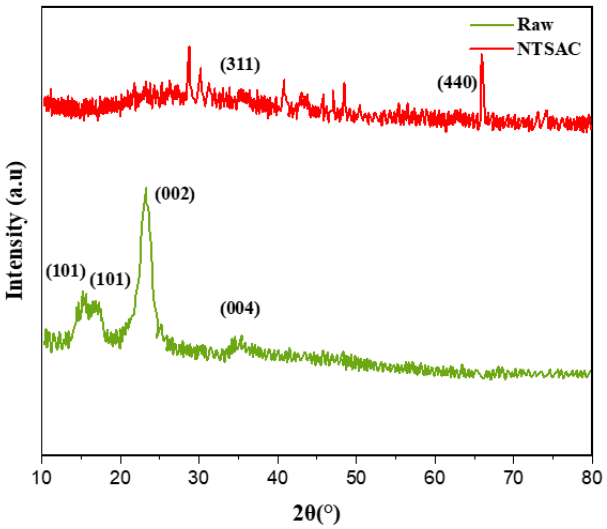

Figure 4. XRD Spectra of raw material and resultant NTSAC sample.

3.1.4. XRD analysis

Figure 4 depicts the XRD spectra of both raw material and NTSAC. Diffraction peaks at 13.60, 17.60, 23.40, and 35.50 in the XRD pattern of raw sample was consistent with cellulose Iβ crystal lattices (101), (101), (200), and (004). The crystalline peaks associated with cellulose, according to Gan and Chow (Gan and Chow 2021), may broaden and flatten when raw particle size decreases, especially below 150 µm. The XRD pattern seen by and NTSAC agreed well with the diffraction peak locations of 18.17, 31.12, 36.25, 42.9, 53.56, 57.41, and 62.98 as reported by Foroutan *et al.* (Foroutan *et al.* 2019). The XRD pattern of AC showed many, overlapping peaks. Biochar made at 450°C from a range of agricultural wastes showed XRD spectra that were very comparable to those of graphite, coquimbite, and hydrobiotite. New peaks at 36.25 and 66.98 were found after biocarbon magnetization, which correlate to magnetite's (311) and (440) lattices. The crystal-like flakes used as decoration for both the raw material and the NTSAC were found to be made primarily of an agglomeration of magnetite nano-crystals, as shown by the XRD profile of the magnetized adsorbents.

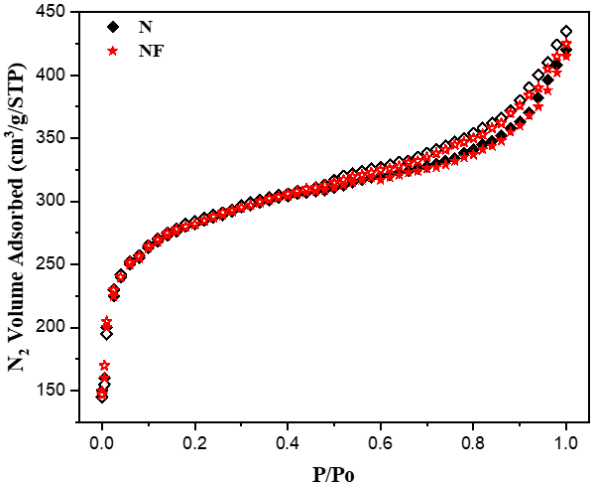

Figure 5. Profiles of N_2 adsorption and desorption for the biocarbon sample before (N) and after magnetization (NF)

The N_2 adsorption-desorption isotherms are illustrated in **Figure 5**. The presence of micropores was indicated by the early section of the isotherms, which was of type I shape (IUPAC classification) for the resultant carbon. In addition, the isotherm displayed a tiny capillary condensation step at high P/P_o values and an H4-type hysteresis loop. According to the results, the presence of both micro-porosity and a tiny part of meso-porosity can be concluded, and the hysteresis loop, found for $P/P_o > 0.5$, can be attributable to capillary condensation in narrow slit-shaped mesopores. Although the amount of N_2 adsorbed at high relative pressure was negligible, this was because of the many mesopores present in the material. Variations in the amount of nitrogen that remains after iron impregnation reflected shifts in textural characteristics. Since iron incorporation may restrict the carbon pores, in this way limiting the surface area of the sorbent and the number of accessible sites for adsorption. Sorbent made from modified carbon should have their surface area quantified for this reason. Pre-magnetization S_{BET} values for AC were found to be 973.65 m^2 g^{-1}, while results for the NTSAC sample showed a modest fall in S_{BET} values, suggesting that iron metal impregnation can cause a drop-in surface area value. The same tendency was observed for V_{tot} and V_{micro} levels. The deposition of iron oxide-based particles, which can fill some of the vacuum spaces of the carbon materials, may be to blame for the reduction in surface area and pore volume. However, the sorption capacity was improved which relates to the sorption sites provided by these iron oxide-based particles.

3.1.5. Thermal characteristics

Thermogravimetric analysis was used to deduce the time-dependent mass change of the adsorbent in relation to the temperature change. The thermographic study of the resultant adsorbent is depicted in **Figure 6**. According to the results, the weight loss in TS biocarbon was observed in four stages: dehydration below 200°C, oxidation of aromatic compounds between 400 and 600°C, carbonate loss between 600 and 800°C, and residual ash breakdown around 800°C. In general, the biocarbon made from various biomasses all go through these phases of weight reduction (Aziz *et al.* 2023). Temperature changes, notably on the upper end, were noticed at the first and third stages of

weight reduction after magnetization. On the other hand, the second phase of weight loss was accompanied with a peak-to-trough change. In magnetized biocarbon, the reduction and volatilization of heavy metals cause a loss of mass between 800 and 900°C.

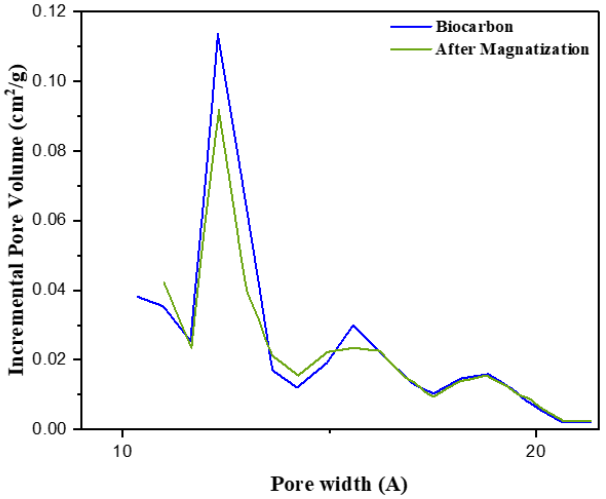

Figure 6. Pore distribution for the biocarbon sample before and after magnetization

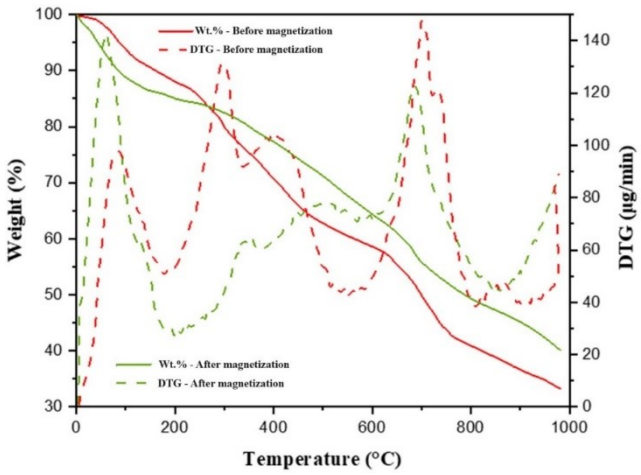

Figure 6. TGA plots of before and after magnetization of biocarbon samples.

3.1.6. Magnetic characteristics

VSM analysis was used to examine the kind of magnetized NTSAC. The ferromagnetic character of the synthesized bio-adsorbent was confirmed by **Figure 7**, which depicts its magnetic hysteresis (M-H) curve. In terms of NTSAC, the values for M_s was determined to be 0.018 emu/g, M_r was 0.004 emu/g, and H_c was 106 O_e. The results were supported by Venkatramanan *et al.* who have examined on magnetized cotton dust biochar (xx). Unwanted contaminants altered the magnitude of the magnetic hysteresis loop in the same way as the crystal lattice's magnetic anisotropy does. While compared to Wang and Zhang report, the hysteresis loop has been significantly reduced due to the presence of non-magnetic crystals such as Fe_3O_4,. The adsorbents' high sensitivity to the magnetic field was established despite their lower magnetic saturation (86-110 emu/g) compared to that of bulk Fe_3O_4 (Wang and Zhang 2020).

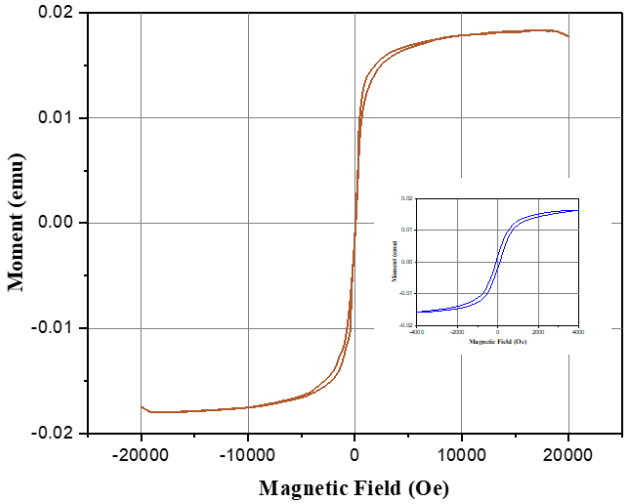

Figure. 7. VSM plots of NTSAC. The insert plot shows an expanded VSM plot with visible hysteresis loop.

3.2. Adsorption of Pb(II) ions by NTSAC

3.2.1. Modeling and optimization analysis for lead (II) ions adsorption

Optimal removal capacities for batch-type adsorption have been calculated using a one-factor-at-a-time method. Based on earlier research, 5 levels were planned for each factor which are highly influencing the adsorption process. To improve the adsorption course parameters and select the best model for the process, the RSM-CCD method was applied. In 30 independently generated CCD experiments, the adsorption was examined as a function of initial Pb(II) concentration (A), dose of NTSAC (B), solution pH (C), and contact time (D). NTSAC exhibited a significant capacity for adsorptive removal of Pb(II) ion, ranging from 16.56 to 92.59 %, from a given solution (**Table 3**). Maximum discrepancy between the model's predicted value and the experiment's actual value was small, suggesting the two were in good agreement. Previous studies on the ability of various activated carbons derived from agricultural waste to remove Pb(II) ions have agreed with the present results (Al-Hazmi *et al.* 2024; Cao *et al.* 2024; Danish *et al.* 2022; Debnath and Das 2023; Mohammadpour *et al.* 2023; Song *et al.* 2013; Zhang *et al.* 2024). The quadratic model was chosen for the RSM statistical modeling development because the predicted and adjusted R^2 values were 0.9524 and 0.9718, respectively, which were the highest that could be achieved. As a result, **Table 4** indicates that, in terms of prediction success, the quadratic model was the best option for the existing configuration.

Table 3. Independent characteristics of the CCD matrix in conjunction with the corresponding experimental and projected response.

Run	Factor 1	Factor 2	Factor 3	Factor 4	Response
	A: Initial Cr (VI) C (mg/L)	B: NTSAC dose g/100 ml	C: pH	D: Contact time (min)	Cr (VI) removal (%)
1	100	3	2.5	150	89.6
2	60	4	3	60	82.52
3	140	2	2	60	80.76
4	140	4	2	120	79.52
5	140	4	2	60	77.67
6	100	3	2.5	90	95.56
7	180	3	2.5	90	69.13
8	100	3	3.5	90	80.82
9	60	2	2	120	91.45
10	100	3	2.5	90	96.56
11	140	2	3	120	77.41
12	60	2	3	60	81.67
13	60	4	3	120	84.15
14	140	4	3	120	72.21
15	100	3	1.5	90	89.12
16	100	3	2.5	90	92.42
17	100	3	2.5	90	94.57
18	100	1	2.5	90	83.54
19	60	2	3	120	86.19
20	140	2	3	60	76.65
21	140	4	3	60	72.98
22	100	3	2.5	90	92.54
23	100	5	2.5	90	77.14
24	100	3	2.5	30	77.69
25	140	2	2	120	88.17
26	60	4	2	120	88.67
27	20	3	2.5	90	84.32
28	100	3	2.5	90	94.65
29	60	4	2	60	80.53
30	60	2	2	60	79.51

Table 4. Statistics of model summery

Source	Sequential p-value	Lack of Fit p-value	Adjusted R^2	Predicted R^2	
Quadratic	< 0.0001	0.9170	0.9718	0.9524	Suggested

Table 5. ANOVA and coefficient of regression for the quadratic model for the adsorptive elimination of Pb(II) ions from aqueous medium using NTSAC

Source	Sum of Squares	df	Mean Square	F-value	p-value	
Model	1580.69	14	112.91	72.49	< 0.0001	significant
A-Initial Cr (VI) Concentration	52.01	1	52.01	33.39	< 0.0001	
B-NTSAC dose	9.70	1	9.70	6.23	0.0247	
C-pH	219.11	1	219.11	140.67	< 0.0001	
D-Contact time	15.31	1	15.31	9.83	0.0068	
AB	19.49	1	19.49	12.51	0.0030	
AC	28.20	1	28.20	18.10	0.0007	
AD	18.02	1	18.02	11.57	0.0039	
BC	0.7396	1	0.7396	0.4748	0.5013	
BD	11.87	1	11.87	7.62	0.0146	
CD	33.64	1	33.64	21.60	0.0003	
A^2	541.27	1	541.27	347.51	< 0.0001	
B^2	343.44	1	343.44	220.50	< 0.0001	
C^2	155.50	1	155.50	99.84	< 0.0001	
D^2	201.78	1	201.78	129.55	< 0.0001	
Residual	23.36	15	1.56			
Lack of Fit	9.88	10	0.9883	0.3665	0.9170	not significant
Pure Error	13.48	5	2.70			
Cor Total	1604.05	29				

Pb(II) removal (%) = - 92.608 + 0.8006 Initial Pb(II) Concentration + 23.984 NTSAC dose + 57.577 pH + 1.041 Contact time - 0.0276 Initial Pb(II) Concentration * NTSAC dose - 0.0664 Initial Pb(II) Concentration * pH - 0.000884 Initial Pb(II) Concentration * Contact time + 0.4300 NTSAC dose * pH - 0.0287 WHAC dose * Contact time - 0.09667 pH * Contact time - 0.00278 Initial Pb(II) Concentratiion² - 3.539 NTSAC dose² - 9.524 pH² - 0.003014 Contact time² (15)

3.3. Statistical analysis

To determine the effect of each process variable on NTSAC's adsorption efficacy towards Pb(II) ions from the solution, an analysis of variance (ANOVA) was performed, and the findings are shown in **Table 5**. When the p-values of the model terms were less than 0.05, the model terms were significant (Kowalczyk *et al.* 2021). Thus, the stated factors and the impact of their interactions affect for the adsorption of Pb(II) ions onto NTSAC were significant, suggesting that the independent components were substantial. In this line, many previous studies on bio-adsorbents made from agricultural waste have reached the same conclusion. With a p-value higher than 0.0001 and an F-value of 82.65, the model showed that the Pb(II) ions adsorption process was well-fitted by the developed model (equation 17).

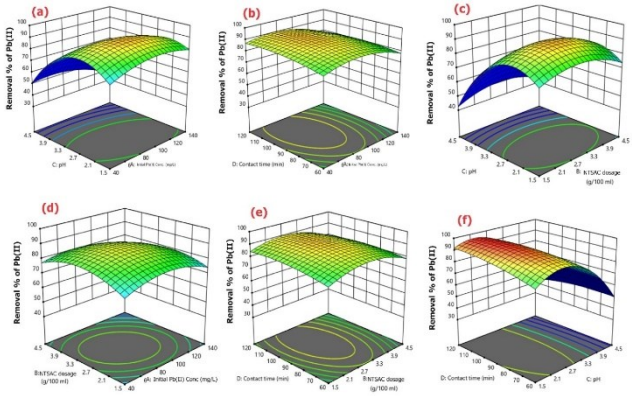

Figure 8. Illustration of interaction effect on the chosen parameters for Pb(II) adsorption.

3.4. Analysis of the effect of parameter interaction on the adsorption process

The current investigation employed the RSM-CCD approach to assess the influence of selected process variables, namely, initial Pb(II) concentration, dose of NTSAC, solution pH, and adsorption time. During examination of interaction effect, the two process components were held constant at their midpoint. The ensuing analysis made with the use of 3D response surface techniques to show the effect of two variables on Pb(II) ion adsorption in an interactive fashion (**Figure 8**). The interaction between adsorbent quantity and Initial Pb(II) concentration was explored in regard to the adsorption of Pb(II) ions from synthetic aqueous medium. The concentration ranges tested were 60 to 170 ppm of Pb(II) and the loading of the adsorbent range was 0.2 to 1 g/100 mL. According to **Figure 8(a)**. Adsorbent dosage of 0.483g/100 mL and starting concentration of 88.87 ppm resulted in a maximum efficacy of 93.41% in Pb(II) ion removal. In contrast, there was no shift in either the adsorption duration or the pH of the solution. Reducing the initial Pb(II) ion concentration and increasing the NTSAC dosage indicate that the adsorption process has been expedited. Since the initial concentration of Pb(II) ions was lower, the increased surface area and number of adsorption sites on the NTSAC account for this result.

This strengthens the connection between the molecule and the NTSAC because the ions are more likely to stick to the empty adsorbent surface. The adsorption rate, however, slowed down with increasing lead molecule concentrations due to site saturation and competition among Lead (II) ions for the finite number of accessible necessary sites. As the initial concentrations of lead ions in aqueous medium via adsorbent increased, the effectiveness of metal removal decreased, according to Khanniri *et al.* in agreement with the findings of this investigation (Khanniri *et al.* 2023). The effectiveness of removing Lead (II) ions was found to be greater than 80% when the adsorbent dosage was increased from 0.2 to 0.8g/100 mL and the initial Pb(II) concentration was raised from 40 to 80 ppm. When Pb(II) concentrations were too high, the active sites necessary for ion adsorption was exhausted. This decreases the adsorbent's overall efficiency. In this vein, Bayuo *et al.* reported on similar experiments (Bayuo *et al.* 2023).

On the following adsorption of Pb(II) ions by NTSAC, the statistical significance of the relationship between initial Pb(II) ion concentration (40-160 ppm) and adsorption period (50-110 min) was evaluated (p = 0.0001). With a modest adsorbent dosage and solution pH, an initial Pb(II) concentration ranging from 45 to 110 ppm, and an adsorbed duration of 40 to 90 min, NTSAC attained an adsorption effectiveness of over 92%. With an initial ion concentration of 88.7 ppm, an adsorb duration of 90 min, and intermediate values of NTSAC dosage and pH value, the maximum Pb(II) absorption efficiency was 94.4%. At lower concentrations of Pb(II) ions, a larger number of ions can be joined to the adsorbent's available surface area because of NTSAC's low dissolved ion to site ratio. Adsorption efficiency decreases with increasing Pb(II) ions concentration, likely because adsorbate compete for a finite number of active sites hence the adsorption sites have become overloaded. **Figure 8(b)** shows that because there were more active sites available during the first stage of contact, the adsorption rate was higher. The entire surface area was filled up as time went on and more Pb(II) ions were adsorbed onto the adsorbent. Şeyda *et al.* have examined on the groundnut shell-based adsorbent to capture Pb(II) ions from the synthetic solution. According to their findings, the adsorbent maintained a steady removal efficiency thereafter, with the peak removal efficiency of 90.26% recorded after 90 min (Taşar *et al.* 2014).

The 3D surface plot of the interaction between the A and C of the solution is illustrated in **Figure 8(c)**. The statistical significance of the interaction effect on Pb(II) removal was supported by a p-value of 0.0425. The solution's pH is a

major influence in the efficiency with which different adsorbents that can remove heavy metals. **Figure 8(c)** illustrates that as the pH of the solution increased from 2 to 5.5, the adsorption process of ions from the medium was boosted. At pH 5.5, NTSAC exhibited its highest capacity for adsorbing Pb(II) ions from aqueous solutions. The adsorption process was less successful at pH values below and above 5.5. Aside from adsorption site competition and solution pH, the net charge of functional groups on the NTSAC surface also influences the ionic state of Pb(II). Media hydrogen ion concentration and the adsorption competition between Pb(II) ions and positive ligand surfaces at low pH were controlled by an anionic binding site on NTSAC's active surface area. This led to reduced electrostatic interaction between the NTSAC particles and Pb(II) ions. However, at high pH levels, the adsorption capacity is reduced by adsorbed hydroxo ions [$Pb(OH)^+$] and/or precipitates of $Pb(OH)_2$ present in the medium. As a result, the NTSAC surfaces have less Pb(II) on them. In such a way, Awual *et al.* observed comparable outcomes, specifying that the optimal solution pH range for removing Pb(II) ions from a synthetic medium was between 2 and 8. Furthermore, they determined that the adsorbent achieved its maximum efficacy in adsorbing Pb(II) ions at a pH of 5.2 (Ghasemi *et al.* 2014).

Figure 8(d) shows the correlation between the lead (II) ion adsorption by NTSAC of the following variables: base concentration, pH of the solution, dose of the adsorbent, and contact/adsorption duration. Using a p-value of 0.0266, the effect of interaction was found to be statistically significant. The results demonstrated that as the concentration of NTSAC increased from 0.2 to 0.8g/100mL and the adsorption time from 50 to 90 minutes, the adsorption process improved. The interaction impact between adsorbent amount and solution pH during the removal of Pb(II) ions is illustrated in **Figure 8(e)**. The significance of their interaction effects was further established by a p-value of 0.0432. According to **Figure 8(f)**, a notable relationship between the adsorption period and solution pH of the media (p-value = 0.0272) was also seen during the lead adsorption process from aqueous media.

3.5. Parametric optimization for maximized removal of Pb(II) ions

In order to ascertain the relevance of the optimization result under the projected optimal points of the CCD design model, triple tests were conducted. **Table 6** presents the adsorption of Pb(II) ions by NTSAC, with the best possible settings for the chosen variables. Removal effectiveness of NTSAC at the ideal concentrations was measured experimentally, and the mean value was very close to the value predicted by the model. This validation therefore demonstrates that the quadratic model was well-appropriate for this procedure.

Table 6. Adsorption of Pb(II) ions by NTSAC, with the best possible settings for the chosen variables

Processing factors	Initial Lead (II) concentration (ppm)	Adsorption time (min)	NTSAC dose (g/100mL)	Solution pH	Removal efficacy (%)		Desirability
					Predicted	Actual	
Optimized conditions	95.355	87.531	0.655	5.6	92.96	90.89	1

Table 7. Comparison of Pb(II) ion adsorption capabilities on different sorbents

Adsorbent	Qmax (mg/g)	References
Fig sawdust	80.64	(Ghasemi *et al.* 2014)
Sawdust of meranti	34.25	(Rafatullah *et al.* 2009)
Carbon obtained from Mentha piperita	53.19	(Ahmad and Haseeb 2017)
Date pits activated carbon	30.70	(Brown *et al.* 2000)
Powder of peanut hull	30.43	(Abdulkarim and Al-Rub 2004)
Waste Algal biomass	44.00	(Vilar *et al.* 2005)
NTSAC	43.97	Present study

Table 8. Linear fit of the isotherm model constants for Pb(II) on NTSAC.

Isotherm model	Factors determined from the linear model fit
Langmuir	k_L = 0.0010943 L/mg; q_m = 73.08 (mg/g); R^2 = 0.985
Freundlich	k_F = 4.052 (mg/g)$(L/mg)^{1/n}$; 1/n = 0.543; R^2 = 0.927
Temkin	k_T = 0.01358; b_T = 165.74; R^2 = 0.936
D-R	q_m = 59.8292; E = 2.914; k_D = 0.0590; R^2 = 0.964

The present study's maximal adsorption capabilities were compared in relation to the results obtained from previous research (**Table 7**). The adsorption of Pb(II) ions was accomplished through the utilisation of adsorbents obtained from several sources of agricultural waste. In comparison to other agricultural waste-based activated carbon, the ABC prepared teff-straw has an adequate importance for Pb(II) ion adsorption (42.97 mg/g).

3.6. Adsorption isotherms

Three isotherm models were used for the examination of the equilibrium data: Dubinin-Radushkevich (D-R), Freundlich (F), and Temkin (T). The outcomes of utilizing equations (5) through (11) to compute the adsorption parameters of the different models are presented in **Table 8**. The manner in which the models forecast the outcomes of the experiments is seen in **Figure 9**. The D-R, F, L, and T isotherm models yielded the R^2 values of 0.985, 0.927, 0.939, and 0.953, respectively, for the NTSAC adsorbent. This demonstrates that, relative to the other models

evaluated, the experimental results were most accurately characterized by the Langmuir (L) isotherm. The nonlinear thermodynamic data, the maximum adsorption capacity, and the fitting parameter (k_L) of the Langmuir model are presented in **Table 8** and **Figure 9**, respectively. According to the L model, the adsorption of sodium ions onto the surface of biomass occurs in a homogeneous and monolayer fashion, suggesting that no interaction has taken place among the Pb(II) ions. Furthermore, separation factor (R_L) which is an additional characteristic of the Langmuir equilibrium model. Theoretically, the isotherm is unfavorable if R_L is greater than one, linear if R_L equals one, reversible if R_L equals zero, and favorable if R_L is less than one. The calculation of the R_L is possible via the subsequent equation (18).

$$R_L = \frac{1}{1 + k_L * C_i} \quad (18)$$

where, C_i initial Pb (II) concentration, k_L is Langmuir constant, and R_L = 0.144.

Because the value of R_L was observed to be between 0 and 1, it is determined that the adsorption of Pb(II) ions was sufficient. Furthermore, it was determined that the highest viable capacity for monolayer adsorption (q_m) was 71.17 mg/g. However, the maximal monolayer adsorption capacity (q_m) of the present bio-adsorbent was marginally greater.

As shown in **Table 8** displays the nonlinear thermodynamic data (k_F), while **Figure 7(b)** displays the fitting parameters (n) for the Freundlich model. Intermolecular adsorption and surface adsorption affinity variation are both modelled by the Freundlich equation for ions adsorbed on heterogeneous surfaces. A pre-established value of n, which denotes the degree of isothermal favorability, and the Freundlich constant (K_F) can be used to compute the adsorption capacity. The equilibrium adsorption of sodium ions onto the bio-sorbent can be described by its adsorption coefficient, k_F. When measuring affinity to a sorbent, a greater k_F value indicates a stronger bond. The heterogeneity of the adsorbent's surface is represented by the Freundlich model parameter n. Leaner absorption occurs when n = 1, while chemical adsorption happens when n > 1, and physical adsorption happens when n < 1. The current bio-adsorbent had a n value of 3.09, suggesting Pb(II) ions were physically adsorbing onto the biomass. However, when compared to the Langmuir model's values, the Freundlich model's R^2 was inadequate. **Figure 9** illustrates the non-linear fitting of the experimental isotherm data to the Temkin isotherm model. R^2 values indicated that the T isotherm model did not appear to well describe the adsorption data. Conversely, the D-R model exhibits a stronger correspondence with the data in relation to the Langmuir isotherm model and was less favorably correlated with the Freundlich and Temkin isotherm models.

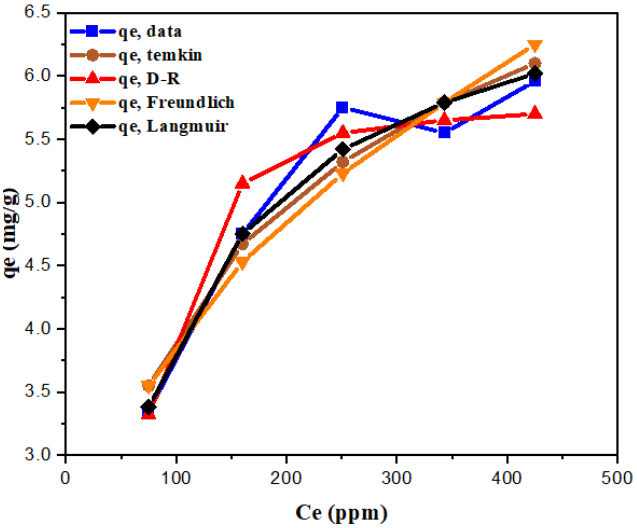

Figure 9. The equilibrium uptake adsorption isotherms for Pb(II) adsorption.

3.7. Adsorption kinetics

The experimental adsorption data was subjected to examine the following kinetic models: pseudo-first-order, second-order, intra-particle diffusion, and Elovich in order to ascertain the rate of Pb(II) adsorption and comprehend the process. Aforementioned models have been employed to fit the experimental findings. The fitting processes' findings are presented in **Table 9**. The observed constants from the fittings of kinetics model were used to depict the adsorption data and the values anticipated by the models stated before (**Figure 10**).

Nevertheless, the R^2 value observed by the pseudo-2nd-order model was 0.999. Experimental data and pseudo-second-order model predictions for q_e for bio-adsorbent were very congruent. This showed that the kinetics data obtained from experimentation for the current biosorbent were best fit by the pseudo-second-order model. A lot of studies have looked at the removal of Pb(II) ions from aqueous media using various adsorbents, and they all exhibited to the same conclusion.

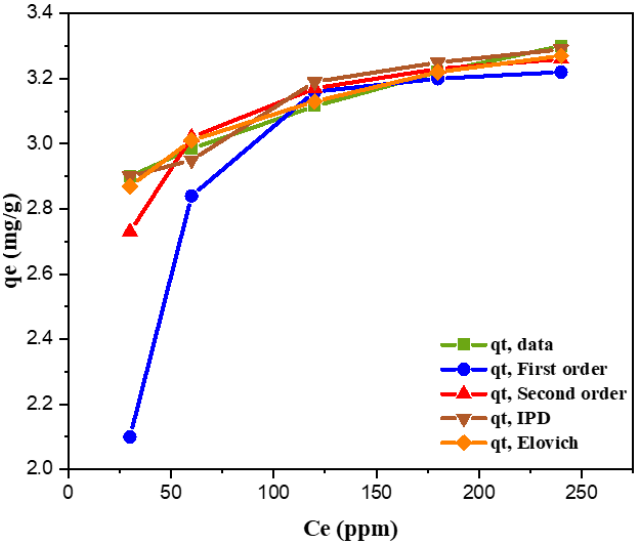

Figure 10. Data fitting to kinetic models of adsorption

Adsorption of Pb(II)ions into the bio-adsorbent was shown to be rate-limiting, and this was determined by testing the intraparticle diffusion model. Depends on intraparticle diffusion kinetic model, R^2 value was calculated to be 0.983; showing the significance of intraparticle diffusion in adsorption. It was apparent that the intraparticle diffusion kinetic model may account for the apparent experimental findings. Comparable in value to the values documented for the adsorptive uptake of additional metal ions from liquids, the intraparticle diffusion rate constant (k_{dif}) was determined to be 0.415 mg/g $mim^{0.5}$. The values of boundary layer thickness (C), which serve as indicators of resistance to external mass transfer, was recorded as 23.971 mg/g. The C values of the present bio-adsorbent for heavy metal removal were similar to those of other bio-adsorbents reported in the scientific literature.

In order to evaluate chemisorption nature of the adsorption process, Elovich kinetic model has been investigated using the adsorption data. In this regard, the R^2 value for the Elovich model's fit to the kinetic data was 0.976. The experimental findings were most well elucidated by the Elovich model, which emphasized the benefits of chemisorption occurring on a heterogeneous surface. Diffusion from the bulk to the surface and chemisorption, in which electrons are shared or exchanged between the adsorbent and the adsorbate, both have a role in regulating the rate at which Pb ions interact with the bio-adsorbent. For the cation interaction with lignocellulose materials, similar fits to isotherms and kinetics were reported from prior investigations.

Table 9. Linear fit kinetic model constants for Pb(II) adsorption on NTSAC.

Kinetic Model	Factors		Kinetic models fitting factors
Pseudo-first order	q_e (mg/g)	Experimental	32.964
		Model	32.154
	k_1 (min^{-1})		0.0353
	R^2		0.784
Pseudo-second order	q_e (mg/g)	Experimental	36.784
		Model	36.599
	k_2 (g/ mg. min.)		0.145
	R^2		0.999
Intra-particle diffusion	k_{dif} (mg/g.$mim^{0.5}$)		0.405
	C (mg/g)		26.708
	R^2		0.983
Elovic	a_E (mg/(g min))		0.517
	b_E (mg/(g min))		164299.1
	R^2		0.966

3.8. Characteristic examination of adsorbent using XPS analysis

XPS tests were conducted on biochar subsequent to sorption in order to delve deeper into the adsorption mechanism. The acquired biocarbon was characterized using X-ray photoelectron spectroscopy (XPS) prior to and subsequent to Pb^{2+} adsorption in order to analyze alterations in the chemical environment and binding energy of the ions under investigation. For C1s, Pb4f, and O1, the survey curves are illustrated in **Figure 11**. According to the results, the maximum binding energies of C-C groups, C-O groups, and O = C-O groups were approximately 285.7 eV, 286.8 eV, and 289.8 eV, respectively. The following peaks were identified: C-O, O-H, and C = O-O at 532.37 eV, 533 eV, and 533.52 eV, respectively; Pb(II) and Pb-O at 140 eV and 142.8 eV, respectively. Following Pb(II) adsorption, the binding energies of these peaks underwent a negligible alteration. As illustrated in **Figure 11(a)**, the adsorbent experiences a reduction in its C-O to C-O ratio due to the adsorption of Pb(II). The morphological changes that occur throughout the adsorption process were shown by the abundance of hydroxyl and carboxyl groups. With the addition of Pb(II), the adsorbed sample's peak areas of O-H and Pb-O increased significantly. A large amount of Pb-O-H was produced during the adsorption process, as shown by the observed changes. Peaks for Pb(II) and Pb-O in the post-adsorption phase show that physical and chemical adsorption occurred during the process.

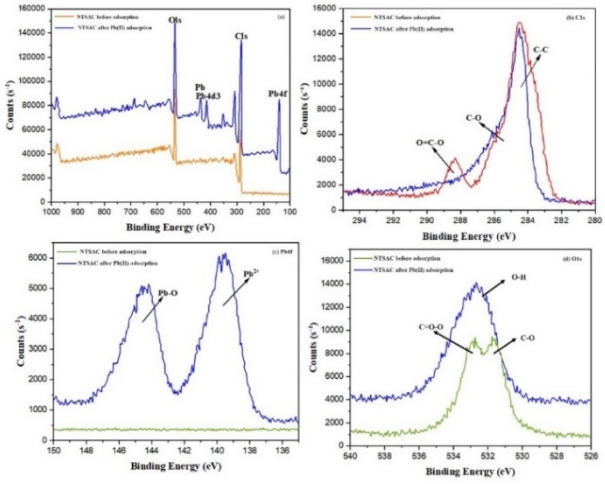

Figure 11. The XPS profiles of biochar before and after adsorption Pb(II)

4. Conclusion

Straw obtained from teff (Eragrostis tef), an annual grass, as a specialty crop of Ethiopia was examined for its ability

to adsorb Pb(II) ions. Nano-scaled magnetized activated carbon (NTSAC) was derived from teff straw and the properties of the NTSAC were ascertained through the use of FTIR, XRD, SEM, BET, and PZC studies. Selective independent factors, such as the initial Pb(II) concentration of, the dose of NTSAC, the solution pH, and the contact time, were optimized using batch adsorption studies employing response surface methods (RSM) in conjunction with CCD matrix. The optimal value from the statistical optimization were as follows: 95.36 mg/L, 0.656 g/100 mL, 5.5, and 88.7 min, respectively. According to isotherms studies, the most precise outcomes were obtained to be well-fitted to the Langmuir isotherm. The kinetic study revealed that the NTASC's Pb(II) ion adsorption rate was found to be suited with the pseudo-second-order model. From the findings, NTSAC exhibits promise as a low-cost bioadsorbent for the removal of harmful Pb(II) ions from contaminated water because it is inexpensively manufactured from locally accessible Ethiopian agricultural waste.

Declarations:

Ethical approval

Not applicable.

Competing interest

Not applicable.

Conflict of interest

The authors declare that they have no conflict of interests.

Consent for publication

All authors agree to the publishing of the paper.

Acknowledgement

The authors express their sincere appreciation to the Researchers Supporting Project number (RSPD2024R679), King Saud University, Riyadh, Saudi Arabia.

Availability of data and materials

Will be provided based on request to corresponding author

Author contributions

M S. Designed experiments, supervised, SB. Wrote initial draft and edited the manuscript, **VS**. carried out investigation, VPS. Validation, characterization and edited the manuscript, SM. wrote initial draft and edited the manuscript, SK. Funding acquisition, and JMK: characterization and software analysis.

Reference

Abdulkarim, M. and Al-Rub, F. A. (2004). Adsorption of lead ions from aqueous solution onto activated carbon and chemically-modified activated carbon prepared from date pits. *Adsorption Science and Technology*, **22**(2), 119–134. https://doi.org/10.1260/026361704323150908

Ahmad, R. and Haseeb, S. (2017). Adsorption of Pb(II) on Mentha piperita carbon (MTC) in single and quaternary systems. *Arabian Journal of Chemistry*, **10**, S412–S421. https://doi.org/10.1016/j.arabjc.2012.09.013

Aiyesanmi, A. F., Adebayo, M. A. and Fadairo, F. F. (2022). Evaluation of avocado pear seed coat for removal of nickel and chromium ions from aqueous solution. *Journal of Hazardous, Toxic, and Radioactive Waste*, **26**(4), 04022027.

Al-Hazmi, G. A. A., El-Zahhar, A. A., El-Desouky, M. G. and El-Bindary, A. (2024). Superior adsorption and removal of doxorubicin from aqueous solution using activated carbon via thermally treated green adsorbent: isothermal, kinetic, and thermodynamic studies. *Environmental Technology (United Kingdom)*, **45**(10), 1969–1988. https://doi.org/10.1080/09593330.2022.2159540

Ameen, M., Zamri, N. M., May, S. T., Azizan, M. T., Aqsha, A., Sabzoi, N. and Sher, F. (2022). Effect of acid catalysts on hydrothermal carbonization of Malaysian oil palm residues (leaves, fronds, and shells) for hydrochar production. *Biomass Conversion and Biorefinery*, **12**, 103–114.

Awad, A. M., Jalab, R., Benamor, A., Nasser, M. S., Ba-Abbad, M. M., El-Naas, M. and Mohammad, A. W. (2020). Adsorption of organic pollutants by nanomaterial-based adsorbents: An overview. *Journal of Molecular Liquids*, **301**, 112335.

Aziz, M. A., Zubair, M., Saleem, M., Alharthi, Y. M., Ashraf, N., Alotaibi, K. S., Aga, O. and Al Eid, A. A. A. (2023). Mechanical, non-destructive, and thermal characterization of biochar-based mortar composite. Biomass Conversion and Biorefinery. https://doi.org/10.1007/s13399-023-03838-1

Bagali, S. S., Gowrishankar, B. S. and Roy, A. S. (2017). Optimization, kinetics, and equilibrium studies on the removal of lead (II) from an aqueous solution using banana pseudostem as an adsorbent. *Engineering*, **3**(3), 409–415.

Balasubramanian, B., Meyyazhagan, A., Chinnappan, A. J., Alagamuthu, K. K., Shanmugam, S., Al-Dhabi, N. A., Ghilan, A. K. M., Duraipandiyan, V. and Arasu, M. V. (2020). Occupational health hazards on workers exposure to lead (Pb): A genotoxicity analysis. *Journal of Infection and Public Health*, **13**(4), 527–531.

Bayuo, J., Rwiza, M. J. and Mtei, K. M. (2023). Non-competitive and competitive detoxification of As(III) ions from single and binary biosorption systems and biosorbent regeneration. *Biomass Conversion and Biorefinery*. https://doi.org/10.1007/s13399-022-03734-0

Beyan, S. M., Ambio, T. A., Sundramurthy, V. P., Gomadurai, C., and Getahun, A. A. (2024). Adsorption phenomenon for removal of Pb (II) via teff straw based activated carbon prepared by microwave-assisted pyrolysis: process modelling, statistical optimisation, isotherm, kinetics, and thermodynamic studies. *International Journal of Environmental Analytical Chemistry*, **104**(4), 916–937.

Brown, P., Atly Jefcoat, I., Parrish, D., Gill, S. and Graham, E. (2000). Evaluation of the adsorptive capacity of peanut hull pellets for heavy metals in solution. *Advances in Environmental Research*, **4**(1), 19–29. https://doi.org/10.1016/S1093-0191(00)00004-6

Cao, S., Cao, J., Zhu, H., Huang, Y., Jin, B. and Materazzi, M. (2024). Removal of HCl from gases using modified calcined Mg-Al-CO3 hydrotalcite: Performance, mechanism, and adsorption kinetics. *Fuel*, **355**, 129445.

Chen, Y., Wang, H., Ying, Z. and Gao, Q. (2020). Ibudilast enhances the clearance of SOD1 and TDP-43 aggregates through TFEB-mediated autophagy and lysosomal biogenesis: The new molecular mechanism of ibudilast and its implication for

neuroprotective therapy. *Biochemical and Biophysical Research Communications*, **526**(1), 231–238.

Dąbrowski, A. (2001). Adsorption—from theory to practice. *Advances in Colloid and Interface Science*, **93**(1–3), 135–224.

Danish, M., Ansari, K. B., Danish, M., Khatoon, A., Rao, R. A. K., Zaidi, S. and Aftab, R. A. (2022). A comprehensive investigation of external mass transfer and intraparticle diffusion for batch and continuous adsorption of heavy metals using pore volume and surface diffusion model. *Separation and Purification Technology*, **292**, 120996.

Debnath, S. and Das, R. (2023). Strong adsorption of CV dye by Ni ferrite nanoparticles for waste water purification: Fits well the pseudo second order kinetic and Freundlich isotherm model. *Ceramics International*, **49**(10), 16199–16215.

Dong, J., Shen, L., Shan, S., Liu, W., Qi, Z., Liu, C. and Gao, X. (2022). Optimizing magnetic functionalization conditions for efficient preparation of magnetic biochar and adsorption of Pb(II) from aqueous solution. Science of the Total Environment, **806**. https://doi.org/10.1016/j.scitotenv.2021. 151442

Duan, R., Chen, Y., Zhou, Y., Long, L., Jiang, Z. and Chen, X. (2023). Adsorption optimization of methylene blue from aqueous solution by cost-effective biochar using response surface methodology and a modeling approach. *Water, Air, & Soil Pollution*, **234**(11), 690.

Foroutan, R., Mohammadi, R., Adeleye, A. S., Farjadfard, S., Esvandi, Z., Arfaeinia, H., Sorial, G. A., Ramavandi, B. and Sahebi, S. (2019). Efficient arsenic(V) removal from contaminated water using natural clay and clay composite adsorbents. *Environmental Science and Pollution Research*, **26**(29), 29748–29762. https://doi.org/10.1007/s11356-019-06070-5

Gan, I. and Chow, W. S. (2021). Tailoring chemical, physical, and morphological properties of sugarcane bagasse cellulose nanocrystals via phosphorylation method. *Journal of Natural Fibers*, **18**(10), 1448–1459. https://doi.org/ 10.1080/15440478.2019.1691120

Ghasemi, M., Naushad, M., Ghasemi, N. and Khosravi-fard, Y. (2014). A novel agricultural waste based adsorbent for the removal of Pb(II) from aqueous solution: Kinetics, equilibrium and thermodynamic studies. *Journal of Industrial and Engineering Chemistry*, **20**(2), 454–461. https://doi.org/10.1016/j.jiec.2013.05.002

Gonçalves, M., Guerreiro, M. C., Oliveira, L. C. A., Solar, C., Nazarro, M. and Sapag, K. (2013a). Micro mesoporous activated carbon from coffee husk as biomass waste for environmental applications. *Waste and Biomass Valorization*, **4**(2), 395–400. https://doi.org/10.1007/s12649-012-9163-1

Gonçalves, M., Guerreiro, M. C., Oliveira, L. C. A., Solar, C., Nazarro, M. and Sapag, K. (2013b). Micro mesoporous activated carbon from coffee husk as biomass waste for environmental applications. *Waste and Biomass Valorization*, **4**, 395–400.

Guel-Nájar, N. A., Rios-Hurtado, J. C., Muzquiz-Ramos, E. M., Dávila-Pulido, G. I., González-Ibarra, A. A. and Pat-Espadas, A. M. (2023). Magnetic biochar obtained by chemical coprecipitation and pyrolysis of corn cob residues: characterization and methylene blue adsorption. *Materials*, **16**(8). https://doi.org/10.3390/ma16083127

Hu, J. and Shipley, H. J. (2012). Evaluation of desorption of Pb (II), Cu (II) and Zn (II) from titanium dioxide nanoparticles. *Science of the Total Environment*, **431**, 209–220.

Huang, J., Cao, Y., Liu, Z., Deng, Z., Tang, F. and Wang, W. (2012). Efficient removal of heavy metal ions from water system by titanate nanoflowers. *Chemical Engineering Journal*, **180**, 75–80.

Igalavithana, A. D., Mandal, S., Niazi, N. K., Vithanage, M., Parikh, S. J., Mukome, F. N. D., Rizwan, M., Oleszczuk, P., Al-Wabel, M. and Bolan, N. (2017). Advances and future directions of biochar characterization methods and applications. *Critical Reviews in Environmental Science and Technology*, **47**(23), 2275–2330.

Ighalo, J. O. and Adeniyi, A. G. (2020). Adsorption of pollutants by plant bark derived adsorbents: an empirical review. *Journal of Water Process Engineering*, **35**, 101228.

Jagadeesh, N. and Sundaram, B. (2023). Adsorption of pollutants from wastewater by biochar: a review. *Journal of Hazardous Materials Advances*, **9**, 100226.

Karuppaiyan, J., Jeyalakshmi, R., Kiruthika, S., Wadaan, M. A., Khan, M. F. and Kim, W. (2023). A study on the role of surface functional groups of metakaolin in the removal of methylene blue: Characterization, kinetics, modeling and RSM optimization. *Environmental Research*, **226**, 115604.

Khanniri, E., Yousefi, M., Mortazavian, A. M., Khorshidian, N., Sohrabvandi, S., Koushki, M. R. and Esmaeili, S. (2023). Biosorption of cadmium from aqueous solution by combination of microorganisms and chitosan: response surface methodology for optimization of removal conditions. *Journal of Environmental Science and Health - Part A Toxic/Hazardous Substances and Environmental Engineering*, **58**(5), 433–446. https://doi.org/10.1080/10934529.2023.2188023

Kifetew, M., Alemayehu, E., Fito, J., Worku, Z., Prabhu, S. V. and Lennartz, B. (2023). Adsorptive removal of reactive yellow 145 dye from textile industry effluent using Teff Straw Activated Carbon: Optimization using central composite design. *Water*, **15**(7), 1281.

Kowalczyk, P., Ligas, B., Skrzypczak, D., Mikula, K., Izydorczyk, G., Witek-Krowiak, A., Moustakas, K. and Chojnacka, K. (2021). Biosorption as a method of biowaste valorization to feed additives: RSM optimization. *Environmental Pollution*, **268**. https://doi.org/10.1016/j.envpol.2020.115937

Kumar, V., Dwivedi, S. K. and Oh, S. (2022). A critical review on lead removal from industrial wastewater: Recent advances and future outlook. *Journal of Water Process Engineering*, **45**, 102518.

Leite, A. B., Saucier, C., Lima, E. C., Dos Reis, G. S., Umpierres, C. S., Mello, B. L., Shirmardi, M., Dias, S. L. P. and Sampaio, C. H. (2018). Activated carbons from avocado seed: optimisation and application for removal of several emerging organic compounds. *Environmental Science and Pollution Research*, **25**, 7647–7661.

Levin, R., Vieira, C. L. Z., Rosenbaum, M. H., Bischoff, K., Mordarski, D. C. and Brown, M. J. (2021). The urban lead (Pb) burden in humans, animals and the natural environment. *Environmental Research*, **193**, 110377.

Merine, M. K., Venkatesa Prabhu, S., Worku, Z., Fito, J. and Alemayehu, E. (2024). Adsorptive removal of reactive yellow 145 dye from textile industry effluents using teff straw-

activated carbon: RSM-based process optimization. *Water Practice & Technology*, **19**(2), 362–383.

Mohammadpour, A., Karami, N., Zabihi, R., Fazeliyan, E., Abbasi, A., Karimi, S., de Farias, M. B., Vieira, M. G. A., Shahsavani, E. and Khaneghah, A. M. (2023). Green synthesis, characterization, and application of Fe3O4 nanoparticles for methylene blue removal: RSM optimization, kinetic, isothermal studies, and molecular simulation. *Environmental Research*, **225**, 115507.

Mohan, D., Kumar, H., Sarswat, A., Alexandre-Franco, M. and Pittman, C. U. (2014). Cadmium and lead remediation using magnetic oak wood and oak bark fast pyrolysis bio-chars. *Chemical Engineering Journal*, **236**, 513–528. https://doi.org/10.1016/j.cej.2013.09.057

Naidu, R., Biswas, B., Willett, I. R., Cribb, J., Singh, B. K., Nathanail, C. P., Coulon, F., Semple, K. T., Jones, K. C. and Barclay, A. (2021). Chemical pollution: A growing peril and potential catastrophic risk to humanity. *Environment International*, **156**, 106616.

Oliveira, L. C. A., Pereira, E., Guimaraes, I. R., Vallone, A., Pereira, M., Mesquita, J. P. and Sapag, K. (2009). Preparation of activated carbons from coffee husks utilizing FeCl3 and ZnCl2 as activating agents. Journal of Hazardous Materials, **165**(1–3), 87–94.

Qasem, N. A. A., Mohammed, R. H. and Lawal, D. U. (2021). Removal of heavy metal ions from wastewater: A comprehensive and critical review. *Npj Clean Water*, **4**(1), 1–15.

Rafatullah, M., Sulaiman, O., Hashim, R. and Ahmad, A. (2009). Adsorption of copper (II), chromium (III), nickel (II) and lead (II) ions from aqueous solutions by meranti sawdust. *Journal of Hazardous Materials*, **170**(2–3), 969–977. https://doi.org/10.1016/j.jhazmat.2009.05.066

Rahman, M. M., Alam, K. and Velayutham, E. (2021). Is industrial pollution detrimental to public health? Evidence from the world's most industrialised countries. *BMC Public Health*, **21**(1), 1175.

Raj, K. and Das, A. P. (2023). Lead pollution: Impact on environment and human health and approach for a sustainable solution. *Environmental Chemistry and Ecotoxicology*, **5**, 79–85.

Rose, P. K., Kumar, R., Kumar, R., Kumar, M. and Sharma, P. (2023). Congo red dye adsorption onto cationic amino-modified walnut shell: Characterization, RSM optimization, isotherms, kinetics, and mechanism studies. *Groundwater for Sustainable Development*, **21**, 100931.

Santhosh, C., Daneshvar, E., Tripathi, K. M., Baltrėnas, P., Kim, T. Y., Baltrėnaitė, E. and Bhatnagar, A. (2020). Synthesis and characterization of magnetic biochar adsorbents for the removal of Cr(VI) and Acid orange 7 dye from aqueous solution. *Environmental Science and Pollution Research*, **27**(26), 32874–32887. https://doi.org/10.1007/s11356-020-09275-1

Sharmiladevi, S., Ramesh, N., Prabhu, S. V. and Mayakannan, S. (2024). Microwave-assisted functionalized biosorbent preparation using seed gum of Tamarindus indica: characterization and evaluation of Cr (VI) removal potency from tannery effluents. *Biomass Conversion and Biorefinery*, 1–13.

Song, M., Jin, B., Xiao, R., Yang, L., Wu, Y., Zhong, Z. and Huang, Y. (2013). The comparison of two activation techniques to prepare activated carbon from corn cob. *Biomass and Bioenergy*, **48**, 250–256. https://doi.org/10.1016/j.biombioe.2012.11.007

Sundramurthy, V. P., Varadharajan, V., Wilson, V. H., Jose, S., Manoharan, S., Alharbi, N. S., Khaled, J. M., Kandasamy, B. and Palanisamy, G. (2024). Adsorptive removal of Cu (II) ions from aqueous solution using Teff (Eragrostis tef) hay based magnetized biocarbon: RSM-GA, ANN based optimization and kinetics aspects. Zeitschrift Für Physikalische Chemie, 0.

Taşar, Ş., Kaya, F. and Özer, A. (2014). Biosorption of lead(II) ions from aqueous solution by peanut shells: Equilibrium, thermodynamic and kinetic studies. *Journal of Environmental Chemical Engineering*, **2**(2), 1018–1026. https://doi.org/10.1016/j.jece.2014.03.015

Tee, G. T., Gok, X. Y. amd Yong, W. F. (2022). Adsorption of pollutants in wastewater via biosorbents, nanoparticles and magnetic biosorbents: A review. *Environmental Research*, **212**, 113248.

Tessema, B., Gonfa, G., Hailegiorgis, S. M. and Prabhu, S. V. (2023). Characteristic investigations on bio-silica gel prepared from teff (eragrostis tef) straw: effect of calcination time. *Materials Research Express*, **10**(11), 115102.

Varadharajan, V., Senthilkumar, D. S., Senthilkumar, K., Sundramurthy, V. P., Manikandan, R., Senthilarasan, H., Ganesan, H., Kesavamoorthy, I. and Ramasamy, A. (2022). Process modeling and toxicological evaluation of adsorption of tetracycline onto the magnetized cotton dust biochar. *Journal of Water Process Engineering*, **49**, 103046.

Vilar, V. J. P., Botelho, C. M. S. and Boaventura, R. A. R. (2005). Influence of pH, ionic strength and temperature on lead biosorption by Gelidium and agar extraction algal waste. *Process Biochemistry*, **40**(10), 3267–3275. https://doi.org/10.1016/j.procbio.2005.03.023

Wang, J. and Zhang, M. (2020). Adsorption characteristics and mechanism of bisphenol a by magnetic biochar. *International Journal of Environmental Research and Public Health*, **17**(3). DOI: 10.3390/ijerph17031075

Zhang, R., Qiao, Q., Liu, T., Zhao, J., Shi, S., Yuan, Y. and Wang, N. (2024). New insights into hydration shells in boosting marine uranium adsorption kinetics. *Chemical Engineering Journal*, **491**, 151995.

Zhao, H., Zhong, H., Jiang, Y., Li, H., Tang, P., Li, D. and Feng, Y. (2022). Porous ZnCl2-activated carbon from shaddock peel: methylene blue adsorption behavior. *Materials*, **15**(3), 895.